Nanoscale

PAPER

View Article Online
View Journal | View Issue

Cite this: *Nanoscale*, 2023, **15**, 12710

Amphiphilic polymeric nanoparticles enable homogenous rhodium-catalysed NH insertion reactions in living cells†

Anjana Sathyan, ‡ Tessa Loman, ‡ Linlin Deng‡ and Anja R. A. Palmans *

Rh-catalysed NH carbene insertion reactions were exported to living cells with help of amphiphilic polymeric nanoparticles. Hereto, hydrophobic dirhodium carboxylate catalysts were efficiently encapsulated in amphiphilic polymeric nanoparticles comprising dodecyl and Jeffamine as side grafts. The developed catalytic nanoparticles promoted NH carbene insertions between α-keto diazocarbenes and 2,3-diaminonaphthalene, followed by intramolecular cyclisation to form fluorescent or biologically active benzoquinoxalines. These reactions were studied in reaction media of varying complexity. The best-performing catalyst was exported to HeLa cells, where fluorescent and cytotoxic benzoquinoxalines were synthesized *in situ* at low catalyst loading within a short time. Most of the developed bioorthogonal transition metal catalysts reported to date are easily deactivated by the reactive biomolecules in living cells, limiting their applications. The high catalytic efficiency of the Rh-based polymeric nanoparticles reported here opens the door to expanding the repertoire of bioorthogonal reactions and is therefore promising for biomedical applications.

Received 1st June 2023,
Accepted 17th July 2023

DOI: 10.1039/d3nr02581k

rsc.li/nanoscale

Introduction

The *in situ* synthesis of bio-active agents is paramount for the development of new innovative therapies. The development of bioorthogonal, new-to-nature reactions is a promising approach and advances in this field have caused a paradigm shift in the field of chemical biology by providing new tools for biomedical research. From studying biomolecules in their native environment to using the same chemistry to release therapeutic drugs directly near tumour sites of human cancer patients, bioorthogonal chemistry has flourished in the past decade.[1–6] Even though some of these bioorthogonal reactions have unprecedented rate, stoichiometric amounts of chemical agents *in vivo* are still required. Introduction of a catalytic component therefore holds great potential, as this can provide signal amplification even at low concentrations. In line with this view, the field has expanded towards transition-metal-catalysed bioorthogonal reactions. These metal catalysts can be thought of as *in situ* chemical "factories" that generate bioactive compounds such as drugs or imaging agents repeatedly from non-toxic starting materials at controlled rates and at a place of interest.[7] However, performing metal catalysis in living environments is a challenging task. The stability of the catalyst is the most important aspect, which must be maintained without compromising the catalyst's activity. Moreover, the catalyst should be biocompatible and ideally water-soluble. Finally, catalysts have to be targeted specifically to the sites of interest.

Both heterogeneous and homogenous bioorthogonal catalysts have been developed in the past decade to meet the beforementioned requirements. This was achieved either by ligand modification or incorporation of the transition metal catalysts (TMCs) in synthetic or natural scaffolds, thereby enabling them to remain in a biological environment and perform reactions.[8–17] Though many studies were successful *in vivo*, the research in this area is still in the early stage. Firstly, this is because often (super)stochiometric amounts of TMCs are required to synthesize bioactive agents in living cells or to activate pro-drugs.[15,18–20] The term 'catalysis' has been used over the years but in the strict definition of the word many of the developed chemistries were not truly 'catalytic'. There are only few examples where real catalytic amounts of TMCs were reported to induce biological activity *in vitro*.[17,21–23] Additionally, so far the focus has mainly been on coupling and cleavage reactions catalysed by commonly used TMCs such as Pd, Cu, Ru and Au in biological media.[8,18,23–30] In order to push the boundaries of the field for biological applications, it important to expand the bioorthogonal toolbox both in terms of developing new and efficient catalysts and thereby new bioorthogonal reactions.

In this regard, metal carbenes are an interesting class of molecules that generate novel bioorthogonal reactions,[31–36]

Institute for Complex Molecular Systems, Laboratory of Macromolecular and Organic Chemistry, Eindhoven University of Technology, P.O. Box 513 Eindhoven, The Netherlands. E-mail: a.palmans@tue.nl

†Electronic supplementary information (ESI) available. See DOI: https://doi.org/10.1039/d3nr02581k

‡These authors contributed equally to this work.

but are less explored in mammalian cell environments. Metal carbenes are formed from diazo compounds and TMCs under mild conditions, making it possible to translate them to water or complex media. Moreover, diazo compounds have been known to endure cell metabolism and were utilized for bioorthogonal reactions *in cellulo*.[37,38] In pioneering work by Mascareñas and co-workers, Cu-catalysed NH carbene insertion reactions were exported to generate bioactive agents *in situ* in HeLa cells.[39] Copper-catalysed reactions are important for proof-of-concept, but their feasibility in biomedical applications may be hindered due to their potential toxicity.[40] Other less toxic metals such as iron, ruthenium, iridium and rhodium also can catalyse NH insertion reactions and are therefore interesting to further explore.[41–46] In particular, rhodium catalysts are attractive for NH carbene insertion reactions in biological media, as they show low toxicity and high stability, where both can be tuned by proper ligand choice.[47] Dirhodium carboxylate catalysts have already been explored to study biological systems exploiting carbene chemistry. Francis and co-workers showed that Rh(II)acetate can catalyse NH insertions to modify tryptophan residues, while Gillingham and co-workers showed the modification of nucleic acids in the same way.[48–50] Previous work in biological environments predominantly focused on the use of water-soluble Rh(II) acetate. However, many hydrophobic dirhodium catalysts have proven to be very reactive towards a wide range of synthetic transformations such as cyclopropanation, C–H and X–H insertion, aromatic substitution and ylide formation reactions in organic solvents.[51] In order to expand their use one has to accommodate for their mostly hydrophobic and thus insoluble character. The catalysts should therefore be solubilized and protected in water-soluble polymeric scaffolds to fully utilize their reactivity in aqueous environments.

An amphiphilic polymer with randomly distributed hydrophobic dodecyl grafts and hydrophilic Jeffamine M-1000 grafts can collapse into single-chain polymeric nanoparticles (SCPNs) in water.[52] These nanometre-sized particles comprise hydrophobic domains in the interior that allow catalyst and substrate accumulation in aqueous solution. Such nanoparticles can be classified to the group of so-called bioorthogonal nanozymes, nanomaterials with enzyme-like properties.[7,53] The nanomaterial scaffolds not only solubilize the catalysts in water, but also protect them from deactivating components in living cells and minimize overall cytotoxicity. They allow substrate accumulation near the catalyst site by the "concentrator effect",[54] enhancing the reaction rate at low concentrations. Further, the cellular uptake of these nanozymes can be modulated by changing the surface functionalities. They hold great promise for *in vivo* applications as they can allow increased circulation times and active targeting if functionalized.[7] Rotello and co-workers have made significant contributions to this field by developing bioorthogonal polyzymes and showing the efficacy of flash nanoprecipitation strategy to increase catalyst loading and turnover frequency.[55–57] Previously in our group, Liu *et al.* explored the potential of these nanoparticles to encapsulate Pd(II) and Cu(I) catalysts to perform bond-cleavage reactions in living cells. However, despite the promising results *in vitro* their catalytic activity was significantly diminished in complex environment due to the presence of deactivating agents.[15] We believe the robust and remarkable activity of dirhodium carboxylates can help us overcome these issues when sequestrated inside our polymeric nanoparticles.

In this work, we investigated the possibility of using Rh carbene chemistry in living cells for the *in situ* synthesis of imaging or bioactive agents with the help of nanomaterial scaffolds, namely amphiphilic polymeric nanoparticles. After selection of the most active catalyst, we performed the annulation of α-keto diazocarbenes with 2,3-diaminonaphthalene in the presence of HeLa cells to form benzoquinoxaline products, a catalytic reaction initiated by an N–H carbene insertion by Rh catalysts following the work of Mascarenas.[39] The results show that quinoxalines readily form using catalytic amounts of Rh embedded in amphiphilic polymeric nanoparticles.

Results and discussion

Encapsulation of dirhodium(II) carboxylate catalysts in amphiphilic polymeric nanoparticles for NH carbene insertion reactions

Dirhodium(II) carboxylates constitute a paddle-wheel-like structure formed by the bridging carboxylate ligands and a unique di-rhodium bridge that offers exceptional stability to these catalysts.[58] Notably, they have two vacant axial positions that allow substrate binding, in this case for carbene formation.[58,59] The hydrophobicity of these catalysts is an important factor to consider when they have to be efficiently encapsulated inside amphiphilic polymeric nanoparticles. Therefore, we chose three highly hydrophobic dirhodium carboxylate catalysts, **C1–C3**, with log *P* values >10 (Fig. 1) for encapsulation. $Rh_2(OAC)_4$, **C4**, has low hydrophobicity (Fig. 1B) and was used as a reference as it is water soluble. Even though **C1–C2** are well studied chiral catalysts, we are only interested in their hydrophobicity, stability and reactivity.

The selected dirhodium carboxylate catalysts **C1–C4** were encapsulated in the hydrophobic interior of a polyacrylamide based amphiphilic polymer **P1** (Fig. 2A and B), which con-

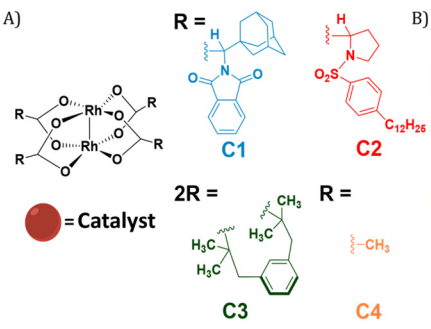

Catalyst	Log P*
C1	11.45
C2	27.05
C3	11.41
C4	2.35

Fig. 1 (A) Chemical structures of dirhodium(II) carboxylates-based catalysts; (B) log *P* values of the catalysts. *calculated using MarvinSketch 22.16.

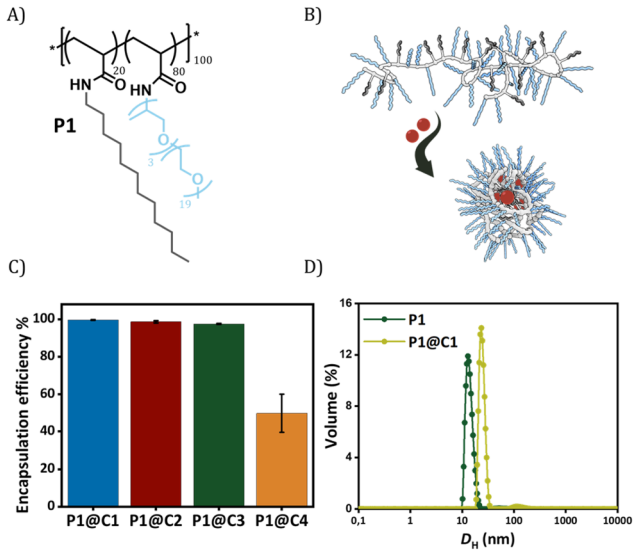

Fig. 2 (A) Chemical structure of amphiphilic random copolymer **P1**, DP = 100, $Đ$ = 1.21; (B) representation of the encapsulation of catalysts **C1–C4** (red spheres) in the hydrophobic interior of polymeric nanoparticles; (C) encapsulation efficiency of the dirhodium carboxylate catalysts **C1–C4** in polymeric nanoparticles calculated from the leached-out rhodium using ICP-OES. [**P1**] = 1 mg mL^{-1}, **P1** : **C** = 1 : 5 (molar ratio), [Rh] = 10 mg L^{-1} before filtration. The results for the encapsulation efficiency are the average of three independent measurements; (D) volume distribution of the hydrodynamic diameter D_H of **P1** and **P1@C1** nanoparticles ([P] = 1.0 mg mL^{-1}, T = 20 °C, [**P1**] : [**C1**] = 1 : 5 (molar ratio)) monitored using DLS measurements.

tained 20% dodecyl grafts for hydrophobicity and 80% Jeffamine M-1000 grafts for hydrophilicity (DP = 100, $Đ$ = 1.21). We chose the simplest design of amphiphilic polymer previously reported by our group that collapsed into SCPNs in water for loading the catalysts.[52] Encapsulation of the catalysts was performed using a modification of a previously reported protocol as described in ESI.†[52]

In order to check the efficiency of **P1** to encapsulate the catalysts, the amount of rhodium that leached out from the nanoparticles was monitored using Inductively Coupled Plasma Optical Emission Spectroscopy (ICP-OES). From here onwards, we represent catalyst encapsulated inside polymeric nanoparticles in solution as **P1@C1–C4**. The solutions of **P1@C1–C4** in water with a total rhodium concentration of 10 mg L^{-1} were filtered using centrifugal filters with a molecular weight cut-off of 50 kDa, to ensure separation of polymeric nanoparticles (MW_{cal} ~ 98 kDa) from the aqueous solution. Therefore, any leached out Rh catalysts (MW = 400–1800 g mol^{-1}) will remain in the filtered solution and the Rh concentration can be monitored using ICP-OES. ICP-OES measurements revealed that for hydrophobic catalysts **C1–C3**, only 0.03–0.2 mg L^{-1} rhodium leached out while in case of hydrophilic catalyst **C4** it was 5 mg L^{-1}. This clearly indicated that the hydrophobic catalysts **C1–C3** were encapsulated with 97–99% efficiency in the hydrophobic interior of **P1** in contrast to hydrophilic catalyst **C4** (50% efficiency) as hypothesized (Fig. 2C).

Dynamic light scattering (DLS) measurements were performed to study the influence of the rhodium encapsulation on the particle size. The hydrodynamic diameter (D_H) of polymeric nanoparticles formed from **P1** without catalysts amounted to ~14 nm (Fig. 2D). For **P1@C1** with a catalyst incorporation ratio of 1 : 5 (**P1** : **C1** molar ratio), D_H increased to ~20 nm, suggesting that the polymeric nanoparticles retain a small size, even after encapsulation of the catalyst. However, the size increase also indicates that there is more than 1 polymer chain present in the nanoparticles, which is why we refer to these systems as "amphiphilic polymeric nanoparticles" instead of "single-chain polymeric nanoparticles". On varying the catalyst incorporation ratio from 1 : 1 to 1 : 10 (**P1** : **C1** molar ratio), a size increase with increasing amount of catalyst encapsulated was observed (for more details see ESI†). We used a ratio of 1 : 5 (**P1** : **C1**) for catalysis studies to keep the polymer concentration low while maintaining high catalyst loading and minimizing aggregation.

Given the successful encapsulation of hydrophobic rhodium catalysts, substrates for the NH carbene insertion reactions were selected as reported earlier by Mascareñas and co-workers (Fig. 3).[39] The diazo substrates **2a–c** were synthesized according to previously reported protocols.[39] The reaction of 2,3-diaminonaphthalene **1** with various diazo substrates **2a–c** affords benzoquinoxalines **3a–c**, by a process initiated by a NH carbene insertion reaction followed by an intramolecular imine condensation and oxidative aromatization (Fig. 3B).[60] The products formed are fluorescent (**3a**) or bioactive (**3c**). Fluorescent benzoquinoxaline **3a** allows visualization of product formation in living cells while **3c** induces cytotoxic effects by promoting mitochondrial fragmentation and depolarization.[39] The *in situ* reaction kinetics can be monitored using fluorescence spectroscopy over time.

Catalytic efficiency of the selected catalysts

P1@C1–C3 were further tested for their efficiency to catalyse the NH carbene insertion reactions, where 2,3-diaminonaphthalene **1** and diazo substrate **2a** were used as substrates. For comparison, hydrophilic catalyst **C4** was used by directly dissolving in water in the absence of polymeric nanoparticles. Reactions were performed at 500 μM concentration of substrates **1** and **2a**, and 10 mol% of catalyst (**C1–C4**) in the appropriate medium (water, PBS and Dulbecco's modified Eagle's medium (DMEM)) at physiological temperature (37 °C). The polymer to catalyst molar ratio

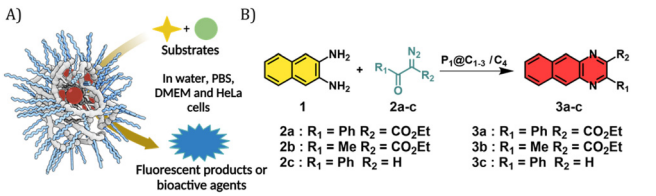

Fig. 3 (A) Representation of reaction involving two substrates using catalytic polymeric nanoparticles; (B) formation of benzoquinoxalines **3a–c** initiated by NH insertion followed by intramolecular cyclisation.

was fixed at 1 : 5 and the concentration of polymer in the reaction mixture was ~1 mg mL^{-1}.

The HPLC-UV chromatogram of the reaction mixture after 24 h indicated that for **P1@C1** diazo substrate **2a** was completely consumed, leading to the formation of product **3a** (Fig. S10A, see ESI†). For **P1@C2** the majority of the substrate **2a** remained in the reaction mixture after 24 h in water (Fig. S10B, see ESI†). **P1@C3** performed better than **P1@C2**, with a significant amount of **3a** formed. However, it was not as efficient as **P1@C1** as full consumption of diazo substrate **2a** was not observed (Fig. S10C, see ESI†). With the hydrophilic catalyst **C4**, a large amount of diazo substrate **2a** remained in the catalytic mixture, and only a negligible amount of product **3a** was formed (Fig. S10D, see ESI†). The consumption of 2,3-diaminonaphthalene **1** was confirmed from the decrease in the fluorescence intensity over time as **1** was not trackable with HPLC-UV (Fig. 4A). Further, the rate of the reaction was calculated from the decrease in fluorescence intensity of 2,3-diaminonaphthalene **1** in the first 180 min (omitting the first 10 min to allow sample equilibration) for **P1@C1–C3** and **C4** (Fig. 4B). The catalytic efficiency followed the order **P1@C1** > **P1@C3** > **P1@C2** > **C4**; the same trend as observed from product formation in the HPLC chromatograms. The hydrophobic catalysts encapsulated in polymeric nanoparticles efficiently catalysed the reaction as compared to free water-soluble catalyst **C4** highlighting the advantage of this system. The hydrophobic domains in these nanoparticles allow substrate solubilisation thereby resulting in the increase in their local concentration near catalytic sites enhancing the rate of reaction. The same results and trends were observed in case of PBS or DMEM as solvent. We did not observe any side product formation such as OH-insertion product or dimerized product from the diazo substrate, which was confirmed by control experiments (for more information see ESI†).

The best performing catalyst **P1@C1** was therefore used for further catalytic studies. As an additional control, we also tested the efficiency of free catalyst **C1** without the presence of amphiphilic polymer but the solution was highly heterogeneous due to high hydrophobicity and conversion was poor when compared to **P1@C1** (Fig. S12, see ESI†). This also highlights the importance of amphiphilic polymeric nanoparticles to achieve homogeneity when exporting these highly active hydrophobic catalysts to biological environment.

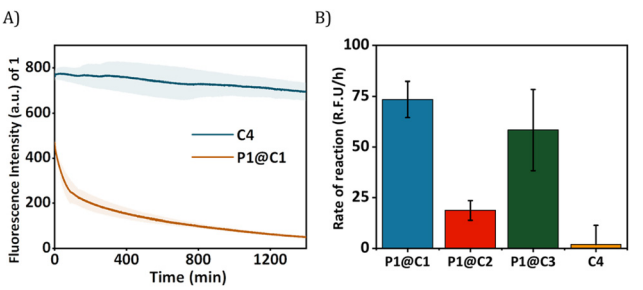

Fig. 4 (A) Fluorescence kinetic profile of reaction progress of **1** and **2a** catalysed by **P1@C1** and **C4** over time, wavy shadows depict the range of error in the kinetic curves, λ_{ex} = 330 nm and λ_{em} = 386 nm; (B) comparison of the rate of the same reaction catalysed by **P1@C1**, **P1@C2**, **P1@C3** and **C4** (t_0 = 10 min and t_F = 180 min); reaction conditions, [**1**] = [**2a**] = 500 μM, [**C**] = 50 μM, [**P**] = 1 mg mL^{-1}, **P1 : C1–C3** = 1 : 5 (molar ratio), T = 37 °C in deionised water. The results are the average of three independent measurements.

Pushing the limits of catalytic efficiency of the best performing catalyst

Reactions were performed under limiting conditions to further test the efficiency of **P1@C1** before exporting it to *in vitro* conditions. Reactions of **1** and **2a** were performed in dilute conditions by lowering the concentration of substrates to 100 μM and 50 μM, respectively, and keeping the amount of catalyst constant at 10 mol% in water. Product formation was observed within 3 h, leading to almost full conversion of **2a** to **3a** within 24 h as evidenced by HPLC-UV (Fig. S11, see ESI†).

Further, the reaction was also performed at 5 mol% of catalyst concentration, which also resulted in significant product formation within 6 h and reaching almost full conversion within 24 h (Fig. S13, see ESI†). Given that the product **3a** was formed with decreased substrate and catalyst concentrations, **P1@C1** proved promising to work under limiting conditions such as dilute concentrations similar to the environment of living cells.

The next step was to further increase the medium complexity and test the efficiency of catalyst in the presence of serum proteins. For this, the same reaction was performed in cell culture medium DMEM supplemented with 10% Fetal Bovine Serum proteins (FBS) with 10 mol% catalyst at 500 μM substrate concentration. The HPLC chromatogram indicated the complete consumption of **2a** and the formation of **3a**. The HPLC chromatogram was compared to a control experiment where **C4** was used as catalyst, which showed no peaks for the product, even after 24 h (Fig. 5A). Notably, the rate of the reaction did not diminish significantly when catalysed by **P1@C1** when medium complexity was increased and the reaction did not proceed in the absence of catalyst (Fig. 5B).

Despite numerous studies and reports on the development of bioorthogonal catalysts, most of the reported catalysts suffer deactivation from nucleophilic attack or get sequestrated by proteins present in complex biological media. This leads to the requirement of high catalyst concentration for reasonable product formation in the presence of cells. In our case, **P1@C1** showed excellent catalytic activity even in the presence of cell culture media and serum proteins at only 10 mol% catalyst concentration and the reaction proceeded to full conversion even at demanding conditions.

Extending the reaction to different diazosubstrates

Given that **P1@C1** proved to be a very efficient catalyst, we examined the substrate scope of these reactions in aqueous media and thereby investigated the possibility to synthesize bioactive molecules in the presence of living cells. We started investigating a NH carbene insertion reaction with very hydro-

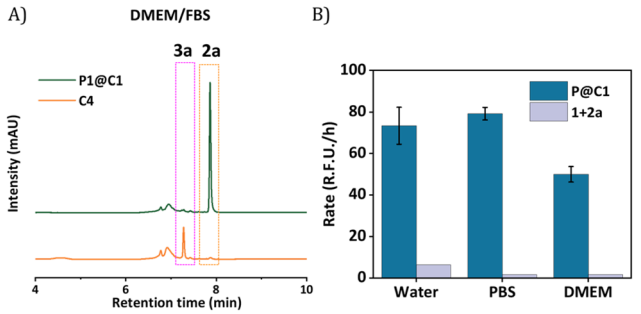

Fig. 5 (A) HPLC-UV chromatogram of the reaction of **1** and **2a** catalysed by **P1@C1**, monitored at 279 nm, [**1**] = [**2a**] = 500 μM in water [**C1**] = 50 μM in DMEM + 10%FBS (unassigned peaks arise from the presence of proteins in FBS in the reaction mixture); (B) comparison of the rate of the same reaction catalysed by **P1@C1** and uncatalysed reaction in water, PBS and DMEM (t_0 = 10 min and t_F = 180 min) determined from fluorescence kinetic measurements. Reaction conditions, [**1**] = [**2a**] = 500 μM, [**C1**] = 50 μM, [**P**] = 1 mg mL^{-1}, **P1** : **C1** = 1 : 5 (molar ratio), T = 37 °C. The results are the average of three independent measurements.

philic diazo substrate **2b** (log P = −2.59) and diamine **1**, which can form benzoquinoxaline **3b**.

In PBS, **P1@C1** showed complete consumption of **2b** and formation of **3b** in 24 h. In case of **C4**, the reaction did not go to completion even though a significant amount of product was formed (Fig. S14, see ESI†). When increasing the medium complexity to DMEM and DMEM/FBS, **C4** did not catalyse the reaction; substrate **2b** remained in the reaction mixture and no product formation was observed (Fig. S14B, see ESI†). Surprisingly for **P1@C1**, there was complete consumption of **2b** but the major product peak **3b** was missing. Instead, a new peak was observed which was found to be the hydrolysed product of **3b** (Fig. S14A and C, see ESI†). We hypothesize that spontaneous hydrolysis of the ester may be brought forward due to the presence of charged groups.[61]

The next substrate investigated was diazo compound **2c**, which can form bioactive cytotoxic compound **3c** as previously described.[39] **P1@C1** showed complete consumption of **2c** and formation of **3c** in 24 h in DMEM and DMEM/FBS (Fig. S16, see ESI†). In case of **C4**, the reaction did not go to completion and a significant amount of **2c** remained in the reaction mixture (Fig. S16, see ESI†).

In short, **P1@C1** is not only efficient, but is also a versatile catalyst that can promote NH carbene insertion reactions in different diazo substrates. The hydrophilic nature of diazo compounds did not hinder metal carbene formation in the presence of polymeric nanoparticles and also did not slow down the reaction as full conversion was obtained within 24 h. It is important to note that in all these reactions, only 10 mol% of catalyst **C1** was used to achieve full conversion irrespective of the medium complexity.

Exporting reactions to living cells

The reactions in cell culture medium such as DMEM and DMEM/FBS confirmed that **P1@C1** is an efficient catalyst and stays catalytically active for prolonged period of time in competitive environments. Furthermore, the fact that only a low catalyst loading is required for complete product conversion made it a promising system to be tested in the presence of living cells. The reaction between **1** and **2a** was chosen as a model reaction as it forms fluorescent benzoquinoxaline **3a** that allows visualization of the product in living cells.[39]

Before performing the catalytic reaction in the presence of cells, the biocompatibility of catalysts **P1@C1** and substrates **2a** and **1** was evaluated. Hereto, HeLa cells were incubated with **P1@C1**, **2a** and **1** separately for 24 h, and at varying concentrations. The CCK-8 assay was then utilized to determine the cell viability. As can be seen in Fig. S19 (see ESI),† the viability of HeLa cells remains above 80% with the increase of **P1@C1** concentration (up to 15 μM), showing good biocompatibility of catalysts. Similarly, cells treated with substrate **2a** in concentrations up to 200 μM exhibit viability above 80% (Fig. S19, ESI†). For substrate **1**, a 24 h incubation with HeLa cells at the concentration of 100 μM caused the cell viability to decrease to around 75%, but by reducing the incubation time to 14 h, cell survival was almost completely restored (Fig. S19, ESI†).

Based on the cytotoxicity study, substrates **1** and **2a** with a concentration of 100 μM were chosen for carrying out the catalytic reaction in the presence of cells. Confocal microscopy was applied to visualize the formed fluorescence product **3a** in cells. To corroborate that product **3a** can only be obtained by catalysing **1** and **2a** using catalyst **P1@C1**, control experiments were performed in which HeLa cells were incubated with only substrates **1+2a**, or one of the substrates (either **1** or **2a**) combined with **P1@C1** (10 mol%); **1+P1@C1** and **2a+P1@C1**. Confocal images of control experiments show that cells incubated with **1+2a** and **1+P1@C1** displayed a low fluorescence signal arising from **1** as it is weakly fluorescent when excited at 405 nm (Fig. 6A and B). Accordingly, **2a+P1@C1** did not show any fluorescence (Fig. 6C). When cells were incubated with **1+2a+P1@C1** for 1.5 h, 3 h and 5 h, the confocal images of the catalytic reactions revealed significant intracellular fluorescence, indicating that product **3a** is formed, notably within even 1.5 h (Fig. 6D). This indicates that the catalytic efficiency of **P1@C1** in the presence of cells is retained and also that the catalyst remains stable. Although it is not clear whether the catalytic reactions occur extracellularly or intracellularly, the most likely scenario is that catalysis occurs extracellularly and that the formed product **3a** diffuses into the cells. The nanoparticles we use here are known to be taken up by endocytosis rather slowly (24 h),[62] and when cells are incubated with quinoxaline **3a**, they become fluorescent, indicating that **3a** can cross the cell membrane (Fig. S20†).

Our next goal was to elicit biological effects in mammalian cells, for which we performed the reaction to form cytotoxic product **3c** from substrates **1** and **2c** in the presence of catalysts **P1@C1**. The cytotoxic product **3c** belongs to a class of molecules known as Tyrphostins (Tyrosin phosphorylation inhibitors), which have distinct biological profiles due to their tyrosine kinase inhibitory activity.[39] To prove that the toxicity originated from product **3c** rather than substrates, product **3c**

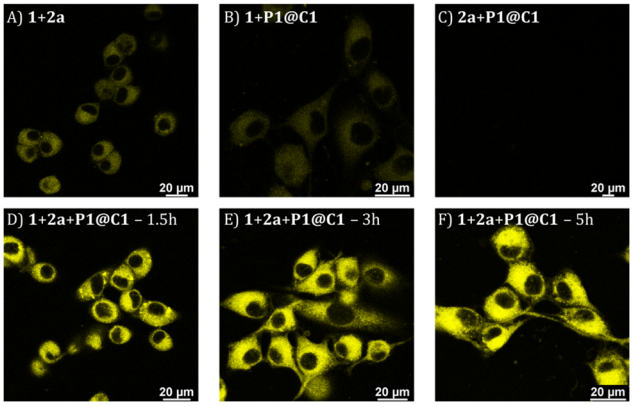

Fig. 6 Confocal microscopy images of HeLa cells incubated with (A) **1+2a** for 5 h; (B) **1+P1@C1** for 5 h; (C) **2a+P1@C1** for 5 h; (D) **1+2a+P1@C1** for 1.5 h; (E) **1+2a+P1@C1** for 3 h; (F) **1+2a+P1@C1** for 5 h; λ_{ex} = 405 nm, λ_{em} = 579–639 nm, [**1**] = [**2a**] = 100 μM and [**C1**] = 10 μM, T = 37 °C, (**P1** : **C1** = 1 : 5 molar ratio).

and substrate **2c** were incubated separately with HeLa cells for their biocompatibility study. After 24 h incubation, the CCK-8 assay demonstrated that substrate **2c** is not toxic to cells; the viability of HeLa cells reaches to 90% (Fig. 7A) under various concentrations (up to 200 μM). In contrast, **3c** treated cells display a viability decrease of 60% (Fig. 7B). A further viability decrease with increasing concentration of **3c** from 25 μM to 100 μM was not observed, indicating the limited capability of **3c** for inducing cell apoptosis.

To test whether **3c** can be synthesized *in situ* in the presence of cells by **P1@C1**, we incubated **1+2c+P1@C1** with HeLa cells and determined the cell viability. Due to the moderate toxicity of **3c**, a high substrate concentration of **1** and **2c** (100 and 200 μM) with catalyst loading of 25 and 50 mol% was used, aimed to generate a sufficient amount of **3c** to induce cell death. A pronounced decrease in cell viability was not observed when the reactions were performed with 100 μM substrates of **1** and **2c** for 14 h (Fig. 7C). However, an increased substrate concentration of 200 μM resulted in the cell viability decreasing to less than 40% after 14 h (Fig. 7C). A low catalyst loading of 25 mol% was found to be sufficient for the efficient synthesis of cytotoxicity compound **3c** *in situ*.

All in all, **P1@C1** proved to be highly catalytically active in the presence of living mammalian cells with superior efficiency leading to the formation of fluorescent and cytotoxic compounds *in situ*. Therefore, it has the potential to be developed as a promising catalyst for biomedical applications as quinoxaline scaffolds are present in many biorelevant compounds.

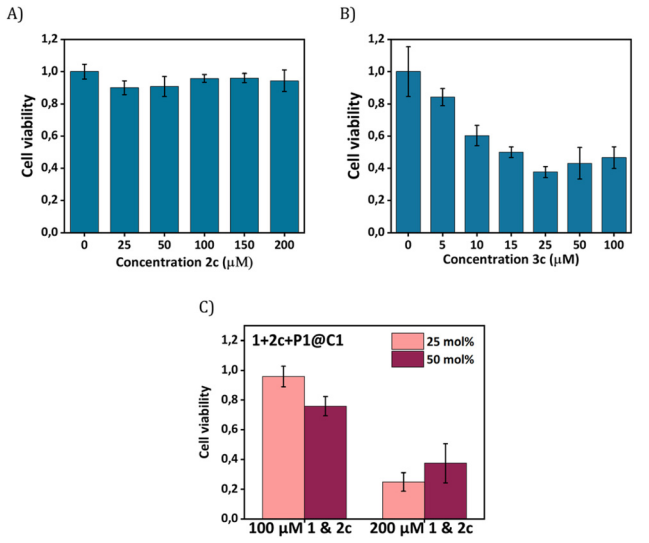

Fig. 7 HeLa cells CCK-8 cell viability assays when incubated with (A) **3c** for 24 h (25–200 μM); (B) **3c** for 24 h (5–100 μM); (C) catalytic reaction **1+2c** (100 & 200 μM) using **P1@C1** (25 and 50 mol% **C1**) in HeLa cells after 14 h.

Conclusions

In conclusion, we found that hydrophobic, stable and highly reactive dirhodium catalysts can be efficiently encapsulated in amphiphilic polymeric nanoparticles. An excellent encapsulation efficiency of 97–99% was observed for hydrophobic catalysts with log P > 10. Among the catalysts screened, **P1@C1** was found to be the best performing and most efficient bioorthogonal catalyst, efficiently catalysing NH carbene insertion reactions between 2,3-diaminonaphthalene and different diazo substrates in aqueous solutions and biologically relevant media. The catalytic efficiency did not change significantly when the complexity of medium was increased from water to cell culture medium with serum proteins. In all cases, complete conversion of substrates to product was observed at 10 mol% catalyst loading within 24 h at low substrate concentrations (<500 μM). To the best of our knowledge, this is the first time highly hydrophobic rhodium catalysts **C1–C2** are utilized to perform NH carbene insertion reactions in homogenous aqueous solution or in the presence of living cells. Although, **C3** and **C4** are already reported to catalyse the same reaction in water, results were obtained at very high substrate concentrations (100 mM) and heterogenous conditions albeit with a reasonable yield of 72% and 38%, respectively.[39] Additionally, this system has advantages over the previously reported copper-catalysed NH carbene insertion reactions *in vitro*, as the use of copper is avoided and micromolar concentrations of substrates are used. Among the three reactions tested, the reaction between **1** and **2b** forming the product **3b** which spontaneously hydrolysed to **3b′** is an excellent example to highlight that polymeric nanoparticles can work in tandem with other catalytic species, likely even with enzymes.

All in all, we presented a highly active and stable catalytic system suitable for NH carbene insertion reactions in very straining conditions by exploiting encapsulation of dirhodium carboxylates in amphiphilic polymeric nanoparticles. The best-performing polymeric nanoparticle catalyst **P1@C1** was exported to HeLa cells where it catalysed the NH carbene inser-

tion reaction to produce photophysically and biologically active products. Importantly, the reactions performed in cells were 'catalytic', which is rarely attained in the case of TMC-catalysed bioorthogonal reactions at low substrate concentrations.

In future, the versatile nature of the dirhodium catalysts can be exploited to further expand the repertoire of efficient bioorthogonal reactions. Additionally, the easy incorporation of different hydrophobic dirhodium catalysts makes the polymeric nanoparticle platform suitable for a wide range of applications including using different TMCs. We anticipate that these studies will drive further advancements in the field, allowing to export new and stable hydrophobic catalysts and reactions to biological environments, leading to new breakthroughs.

Author contributions

This manuscript was written through the contributions of all authors. All authors have given approval to the final version of manuscript.

Conflicts of interest

There are no conflicts to declare.

Acknowledgements

This work is financed by the European Union's Horizon 2020 Research and Innovation Program under the Marie Sklodowska-Curie Grant Agreement No. 765497 (THERACAT).

References

1 N. J. Agard, J. A. Prescher and C. R. Bertozzi, *J. Am. Chem. Soc.*, 2004, **126**, 15046–15047.
2 C. R. Bertozzi, *Acc. Chem. Res.*, 2011, **44**(9), 651–653.
3 Phase 1/2a Study of SQ3370 in Patients With Advanced Solid Tumors – ClinicalTrials.gov, 5 February 2023.
4 J. M. M. Oneto, I. Khan, L. Seebald and M. Royzen, *ACS Cent. Sci.*, 2016, **2**, 476–482.
5 K. Wu, N. A. Yee, S. Srinivasan, A. Mahmoodi, M. Zakharian, J. M. Mejía Oneto and M. Royzen, *Chem. Sci.*, 2021, **12**, 1259–1271.
6 S. Srinivasan, N. A. Yee, K. Wu, M. Zakharian, A. Mahmoodi, M. Royzen and J. M. Mejía Oneto, *Adv. Ther.*, 2021, **4**, 2000243.
7 S. Fedeli, J. Im, S. Gopalakrishnan, J. L. Elia, A. Gupta, D. Kim and V. M. Rotello, *Chem. Soc. Rev.*, 2021, **50**, 13467–13480.
8 M. A. Miller, B. Askevold, H. Mikula, R. H. Kohler, D. Pirovich and R. Weissleder, *Nat. Commun.*, 2017, **8**, 1–13.
9 M. A. Miller, H. Mikula, G. Luthria, R. Li, S. Kronister, M. Prytyskach, R. H. Kohler, T. Mitchison and R. Weissleder, *ACS Nano*, 2018, **12**, 12814–12826.
10 A. M. Pérez–López, B. Rubio–Ruiz, V. Sebastián, L. Hamilton, C. Adam, T. L. Bray, S. Irusta, P. M. Brennan, G. C. Lloyd–Jones, D. Sieger, J. Santamaría and A. Unciti–Broceta, *Angew. Chem.*, 2017, **129**, 12722–12726.
11 R. M. Yusop, A. Unciti-Broceta, E. M. V. Johansson, R. M. Sánchez-Martín and M. Bradley, *Nat. Chem.*, 2011, **3**, 239–243.
12 J. Chen, J. Wang, K. Li, Y. Wang, M. Gruebele, A. L. Ferguson and S. C. Zimmerman, *J. Am. Chem. Soc.*, 2019, **141**, 9693–9700.
13 J. Chen, J. Wang, Y. Bai, K. Li, E. S. Garcia, A. L. Ferguson and S. C. Zimmerman, *J. Am. Chem. Soc.*, 2018, **140**, 13695–13702.
14 Y. Bai, X. Feng, H. Xing, Y. Xu, B. K. Kim, N. Baig, T. Zhou, A. A. Gewirth, Y. Lu, E. Oldfield and S. C. Zimmerman, *J. Am. Chem. Soc.*, 2016, **138**, 11077–11080.
15 Y. Liu, S. Pujals, P. J. M. Stals, T. Paulöhrl, S. I. Presolski, E. W. Meijer, L. Albertazzi and A. R. A. Palmans, *J. Am. Chem. Soc.*, 2018, **140**, 3423–3433.
16 K. Tsubokura, K. K. H. Vong, A. R. Pradipta, A. Ogura, S. Urano, T. Tahara, S. Nozaki, H. Onoe, Y. Nakao, R. Sibgatullina, A. Kurbangalieva, Y. Watanabe and K. Tanaka, *Angew. Chem., Int. Ed.*, 2017, **56**, 3579–3584.
17 S. Learte-Aymamí, C. Vidal, A. Gutiérrez-González and J. L. Mascareñas, *Angew. Chem., Int. Ed.*, 2020, **59**, 9149–9154.
18 J. Konč, V. Sabatino, E. Jiménez-Moreno, E. Latocheski, L. R. Pérez, J. Day, J. B. Domingos and G. J. L. Bernardes, *Angew. Chem., Int. Ed.*, 2022, **61**, e202113519.
19 Y. Bai, J. Chen and S. C. Zimmerman, *Chem. Soc. Rev.*, 2018, **47**, 1811–1821.
20 J. G. Rebelein and T. R. Ward, *Curr. Opin. Biotechnol.*, 2018, **53**, 106–114.
21 M. A. Miller, B. Askevold, H. Mikula, R. H. Kohler, D. Pirovich and R. Weissleder, *Nat. Commun.*, 2017, **8**, 1–13.
22 T. Völker, F. Dempwolff, P. L. Graumann and E. Meggers, *Angew. Chem., Int. Ed.*, 2014, **53**, 10536–10540.
23 T. Völker and E. Meggers, *ChemBioChem*, 2017, **18**, 1083–1086.
24 J. Chen, J. Wang, K. Li, Y. Wang, M. Gruebele, A. L. Ferguson and S. C. Zimmerman, *J. Am. Chem. Soc.*, 2019, **141**, 9693–9700.
25 A. M. Pérez-López, B. Rubio-Ruiz, V. Sebastián, L. Hamilton, C. Adam, T. L. Bray, S. Irusta, P. M. Brennan, G. C. Lloyd-Jones, D. Sieger, J. Santamaría and A. Unciti-Broceta, *Angew. Chem., Int. Ed.*, 2017, **56**, 12548–12552.
26 P. Destito, A. Sousa-Castillo, J. R. Couceiro, F. López, M. A. Correa-Duarte and J. L. Mascareñas, *Chem. Sci.*, 2019, **10**, 2598–2603.
27 A. Unciti-Broceta, E. M. V. Johansson, R. M. Yusop, R. M. Sánchez-Martín and M. Bradley, *Nat. Protoc.*, 2012, **7**, 1207–1218.

28 M. C. Ortega–Liebana, N. J. Porter, C. Adam, T. Valero, L. Hamilton, D. Sieger, C. G. Becker and A. Unciti–Broceta, *Angew. Chem.*, 2022, **134**, e202111461.
29 A. M. Pérez-López, A. Belsom, L. Fiedler, X. Xin and J. Rappsilber, *J. Med. Chem.*, 2023, **66**, 3301–3311.
30 C. Adam, T. L. Bray, A. M. Pérez-López, E. H. Tan, B. Rubio-Ruiz, D. J. Baillache, D. R. Houston, M. J. Salji, H. Y. Leung and A. Unciti-Broceta, *J. Med. Chem.*, 2022, **65**, 552–561.
31 T. G. Rajagopalan, W. H. Stein and S. Moore, *J. Biol. Chem.*, 1966, **241**, 4295–4297.
32 D. M. Carminati and R. Fasan, *ACS Catal.*, 2019, **9**, 9683–9697.
33 M. C. M. van Oers, L. K. E. A. Abdelmohsen, F. P. J. T. Rutjes and J. C. M. van Hest, *Chem. Commun.*, 2014, **50**, 4040–4043.
34 Z. J. Wang, H. Renata, N. E. Peck, C. C. Farwell, P. S. Coelho and F. H. Arnold, *Angew. Chem., Int. Ed.*, 2014, **53**, 6810–6813.
35 K. Chen, S. Q. Zhang, O. F. Brandenberg, X. Hong and F. H. Arnold, *J. Am. Chem. Soc.*, 2018, **140**, 16402–16407.
36 S. Wallace and E. P. Balskus, *Angew. Chem., Int. Ed.*, 2015, **54**, 7106–7109.
37 K. A. Mix, M. R. Aronoff and R. T. Raines, *ACS Chem. Biol.*, 2016, **11**, 3233–3244.
38 K. A. Andersen, M. R. Aronoff, N. A. McGrath and R. T. Raines, *J. Am. Chem. Soc.*, 2015, **137**, 2412–2415.
39 S. Gutiérrez, M. Tomás–Gamasa and J. L. Mascareñas, *Angew. Chem.*, 2021, **133**, 22188–22196.
40 E. M. Sletten and C. R. Bertozzi, *Angew. Chem., Int. Ed.*, 2009, **48**, 6974–6998.
41 K. Ramakrishna and C. Sivasankar, *Org. Biomol. Chem.*, 2017, **15**, 2392–2396.
42 D. Gillingham and N. Fei, *Chem. Soc. Rev.*, 2013, **42**, 4918.
43 B. J. Anding and L. K. Woo, *Organometallics*, 2013, **32**, 2599–2607.
44 A. Rioz-Martínez, J. Oelerich, N. Ségaud and G. Roelfes, *Angew. Chem., Int. Ed.*, 2016, **55**, 14136–14140.
45 H. F. Srour, P. Le Maux, S. Chevance, D. Carrié, N. Le Yondre and G. Simonneaux, *J. Mol. Catal. A: Chem.*, 2015, **407**, 194–203.
46 A. M. Abu-Elfotoh, *Tetrahedron Lett.*, 2017, **58**, 4750–4754.
47 M. B. Minus, M. K. Kang, S. E. Knudsen, W. Liu, M. J. Krueger, M. L. Smith, M. S. Redell and Z. T. Ball, *Chem. Commun.*, 2016, **52**, 11685–11688.
48 J. M. Antos, J. M. Mcfarland, A. T. Iavarone and M. B. Francis, *J. Am. Chem. Soc.*, 2009, **131**(17), 6301–6308.
49 J. M. Antos and M. B. Francis, *J. Am. Chem. Soc.*, 2004, **126**, 10256–10257.
50 K. Tishinov, K. Schmidt, D. Häussinger and D. G. Gillingham, *Angew. Chem., Int. Ed.*, 2012, **51**, 12000–12004.
51 J. P. Snyder, A. Padwa and T. Stengel, *J. Am. Chem. Soc.*, 2001, **123**, 11318–11319.
52 G. M. ter Huurne, L. N. J. de Windt, Y. Liu, E. W. Meijer, I. K. Voets and A. R. A. Palmans, *Macromolecules*, 2017, **50**, 8562–8569.
53 Z. Zhang and K. Fan, *Nanoscale*, 2022, **15**, 41–62.
54 B. Helms, C. O. Liang, C. J. Hawker and J. M. J. Fréchet, *Macromolecules*, 2005, **38**, 5411–5415.
55 R. Huang, C. M. Hirschbiegel, X. Zhang, A. Gupta, S. Fedeli, Y. Xu and V. M. Rotello, *ACS Appl. Mater. Interfaces*, 2022, **14**, 31594–31600.
56 X. Zhang, R. F. Landis, P. Keshri, R. Cao-Milán, D. C. Luther, S. Gopalakrishnan, Y. Liu, R. Huang, G. Li, M. Malassiné, I. Uddin, B. Rondon and V. M. Rotello, *Adv. Healthcare Mater.*, 2021, **10**, 2001627.
57 C. M. Hirschbiegel, S. Fedeli, X. Zhang, R. Huang, J. Park, Y. Xu and V. M. Rotello, *Materials*, 2022, **15**, 6487.
58 F. G. Adly, *Catalysts*, 2017, **7**, 347.
59 M. P. Doyle, *J. Org. Chem.*, 2006, **71**, 9253–9260.
60 R. P. Pandit, S. H. Kim and Y. R. Lee, *Adv. Synth. Catal.*, 2016, **358**, 3586–3599.
61 D. J. Blevins, R. Nazir, S. M. H. Dabiri, M. Akbari and J. E. Wulff, *J. Drug Delivery Sci. Technol.*, 2022, **78**, 103950.
62 L. Deng, L. Albertazzi and A. R. A. Palmans, *Biomacromolecules*, 2022, **23**, 326–338.